# Synthesis, Structural, and Optical Properties of Stable ZnS:Cu,Cl Nanocrystals†

**Carley Corrado,‡ Yu Jiang,§ Fadekemi Oba,‡ Mike Kozina,§ Frank Bridges,*,§ and Jin Z. Zhang*,‡**

*Department of Chemistry and Biochemistry and Department of Physics, University of California, Santa Cruz, California 95064*

*Received: November 1, 2008; Revised Manuscript Received: December 9, 2008*

Stable water-suspendable $Cu^+$-doped ZnS nanocrystals (NCs) have been synthesized with mercaptopropionic acid (MPA) as a capping molecule. The nanocrystals have been characterized using a combination of experimental techniques including UV−vis and photoluminescence (PL) spectroscopy, X-ray diffraction (XRD), transmission electron microscopy (TEM), inductively coupled plasma (ICP), and extended X-ray absorption fine structure (EXAFS). The UV−vis electronic absorption spectrum shows an excitonic peak at 310 nm, characteristic of quantum-confined ZnS NCs. This excitonic peak does not change noticeably with $Cu^+$ doping. XRD confirms the formation of ZnS nanocrystals, and the average size of the NCs has been determined to be around 6 nm by TEM. The incorporation of $Cu^+$ into the ZnS is manifested as a substantial red-shift of the emission band in the PL spectra upon addition of $Cu^{2+}$ that was reduced into $Cu^+$ during the synthesis reaction. EXAFS data were obtained to confirm copper doping as well as determine the local structure about $Cu^+$ and $Zn^{2+}$ in the NCs. Fitting to the EXAFS data for $Cu^+$ suggests that most $Cu^+$ ions are located near the surface within the ZnS NCs and that a significant fraction may be in the form of CuS as found in bulk material. These combined optical and structural studies have provided important new insight into the relevant electronic energy levels and their correlation to the optical and structural properties of ZnS:Cu,Cl NCs. This has important implications in potential applications of this phosphor material for solid state lighting, imaging, and other photonic devices.

## 1. Introduction

In recent years, semiconductor nanocrystals (NCs) have drawn significant attention due to their unique structural, electronic, and optical properties originating from their large surface-to-volume (S/V) ratio and quantum confinement effect.[1−13] An important subset of semiconductor NCs are those doped with a small percentage of dopants to alter their electronic, magnetic, and optical properties for various desired applications.[14−25] One of the promising applications of doped semiconductor NCs is solid state lighting based on AC electroluminescent (EL) devices that are expected to have high electrical-to-light conversion efficiency.[26−32]

Cubic ZnS with a bulk bandgap of 3.7 eV is a common and attractive choice as a host semiconductor for doping to produce nanophosphors in EL applications due to its stability, low cost, and low toxicity.[26,27,30,32−36] A number of metal ions, such as $Mn^{2+}$, $Cu^+$, $Pb^{2+}$, $Ag^+$, and $Eu^{2+}$, have been successfully doped into ZnS to produce PL or EL emission in different regions of the visible spectrum.[37−48] Compared to bulk or micrometer scale powders, these nanoscale materials are anticipated to have some unique properties that are potentially useful to improve their AC EL performance, for example, in terms of efficiency and required voltage.[20] In EL applications, AC is preferred since the AC voltage required is usually 2 orders of magnitude lower than for DC voltages.

Currently, one major limitation in AC EL devices is that the material degrades when subjected to high AC electric fields ($\sim 10^6$ V/m), but the degradation mechanism is still not well understood.[32] There are also unresolved fundamental questions regarding the structure of the nanophospors and the luminescence mechanism. For example, in bulk ZnS:Cu,Cl, the mechanism for light emission proposed by Fischer involves localized electron and hole injection near conducting CuS precipitates which form for Cu concentrations > 400 ppm.[49] In these materials Cu is only in the +1 valence state unless excited optically.[50] The emission is caused by recombination of an electron and a hole, associated with $Cl^-$ and $Cu^+$ levels, respectively. However, there have been different models or explanations about the AC EL mechanism and the associated electronic energy levels of the host (ZnS) and dopant ions.[51]

Traditionally, these AC EL devices have been made using micrometer-sized phosphor particles. Recently, there has been considerable interest in using nanophosphors for EL application since they can potentially allow fabrication of thinner, smaller, and ideally more efficient devices. Since the electric field is inversely proportional to the thickness, $d$, of the device ($E = V/d$), an equivalent large electric field could be achieved for a thin device for a low applied voltage. Control of NC size and shape as well as doping could be used to engineer devices that could withstand higher electric fields without degradation. The first step toward this goal is to have a detailed understanding of the electronic energy levels of the dopant, $Cu^+$, and their relation to the structural and optical properties in the host semiconductor, ZnS.

Before detailed AC EL studies are conducted, it is often helpful to study the PL properties since a PL measurement is more convenient to carry out and provides important information about the energy levels relevant to EL. In conjunction with structural studies, PL studies allow us to gain insight into the

† Part of the "George C. Schatz Festschrift".

* Corresponding authors. E-mail: bridges@physics.ucsc.edu, zhang@chemistry.ucsc.edu.

‡ Department of Chemistry and Biochemistry.

§ Department of Physics.

10.1021/jp809666t CCC: $40.75 
Published on Web 01/26/2009

correlation between optical and structural properties through the associated energy levels. Toward this goal, it is necessary to conduct structural studies together with optical characterizations. One powerful structural characterization method is extended X-ray absorption fine structure (EXAFS), which probes the local structures around the center atom or ion.[52] There are basically two types of data collection methods in EXAFS: transmission and fluorescence. For samples where the center atoms have relatively high concentrations, the transmission measurement is normally applied. If the concentration is low, a fluorescence measurement is used since it is more sensitive. To our best knowledge, no EXAFS studies have been reported on ZnS:Cu,Cl NCs to date.

In this paper, we report the synthesis of stable and luminescent ZnS:Cu,Cl NCs through a modified and improved synthetic method. Using a combination of experimental techniques, the optical and structural properties of these NCs were characterized in detail to shed light on some of the issues mentioned above. Through combined optical and structural studies, the results obtained are used to refine the energy levels involved and to explain the PL observed, with emphasis on correlating the relevant energy levels of interest with the local structure of the Cu dopant in ZnS NCs.

## 2. Experimental Section

**2.1. Materials.** All the chemicals were of reagent grade and used without further purifications. 3-Mercaptopropionic acid (MPA, #107-96-0, 99+% purity) and sodium hydroxide (NaOH, #1310-73-2, 98.5% purity) were purchased from Acros Organics (Morris Plains, NJ). Zinc nitrate hexahydrate ($Zn(NO_3)_2 \cdot 6H_2O$, #10196-18-6, crystalline/certified) was purchased from Fisher Scientific (Pittsburgh, PA). Copper(II) chloride dihydrate ($CuCl_2 \cdot 2H_2O$, #10125-13-0, 99+% purity) was purchased from Sigma-Aldrich (Milwaukee, WI). Sulfur powder (#7704-34-9, 99.999% purity) was Puratronic, purchased from Alfa Aesar (Ward Hill, MA). High purity (>18 Ω cm) Milli-Q water (Millipore, Watford) was used.

**2.2. Synthesis.** ZnS:Cu,Cl nanocrystals with various Cu concentrations were synthesized via an aqueous route similar to Zhuang's method for ZnS:Mn.[53] For 1% copper doping, the synthesis is as follows. In a three-neck round-bottomed flask, 5 mL of 0.1 M $Zn(NO_3)_2 \cdot 6H_2O$, 0.850 mL of 0.00587 M $CuCl_2 \cdot 2H_2O$, and 20 mL of 0.1 M MPA were combined. This solution was diluted to 45.5 mL with water, and the pH was adjusted to ~11 using 2 M NaOH. Next the solution was degassed by bubbling $N_2$ gas for 30 min, after which 4.5 mL of degassed 0.1 M $Na_2S \cdot 9H_2O$ was quickly injected into the solution. It remained clear and was stirred for 15 min. Stock solutions of $Zn(NO_3)_2 \cdot 6H_2O$ and $CuCl_2 \cdot 2H_2O$ were prepared and used for many syntheses. MPA and $Na_2S \cdot 9H_2O$ solutions were less stable and prepared fresh each time the synthesis was performed.

The reaction mixture was then exposed to air, and UV−vis was taken to confirm formation of NCs. The crude solution showed no luminescence. It was refluxed 1 h, then 3.8 mL of 0.1 M $Zn(NO_3)_2 \cdot 6H_2O$ was injected into the reaction, and finally the solution was refluxed another hour.

The NCs were precipitated from solution by addition of ~22 mL of ethanol (water to ethanol of 2:1). The solution was centrifuged at 3000 rpm for 20 min at room temperature. The supernatant was discarded, and the precipitated NCs were washed 3 more times with ethanol (~10 mL). The NCs were then suspended, or "dissolved", in water (1−2 mL) to yield a clear solution, which was lyophilized to become a white fluffy powder that is suspendable in water. This powder was then used for XRD, ICP, EXAFS, and TEM measurements.

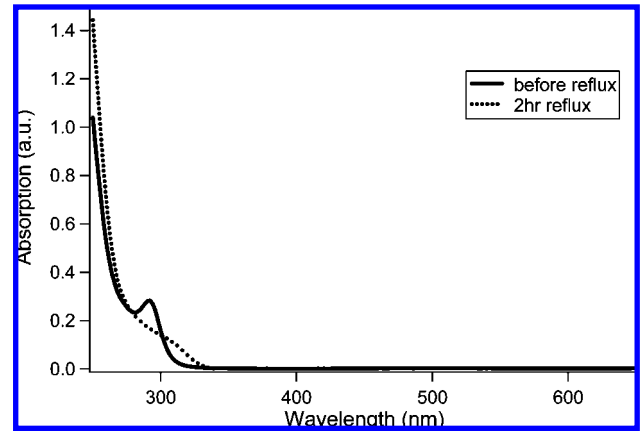


**Figure 1.** UV−visible electronic absorption spectra of ZnS:Cu,Cl colloidal NCs before and after reflux.

**2.3. Instrumentation.** The crystal structure of the samples was characterized by X-ray diffraction (XRD, Rigaku Americas Miniflex Plus powder diffractometer), using Cu Kα ($\lambda$ = 1.54056 Å) irradiation. Diffraction patterns were recorded from 20 to 80 $2\theta$, with a step size of 0.04° at a rate of 2° per minute. The UV−vis absorption spectra were taken on a Hewlett-Packard 8452A diode array spectrophotometer at room temperature. The photoluminescence (PL) and photoluminescence excitation (PLE) spectra were measured on a Perkin-Elmer luminescence spectrometer LS50B at room temperature. The samples that were analyzed with spectrophotometry were prepared by dispersing the nanoparticles in Milli-Q water, basified to pH ~ 11 with NaOH, to yield a clear solution. Centrifugation was performed on a Sorvall Legend RT at 3000 rpm for 20 min at room temperature. The Cu concentrations were determined using inductively coupled plasma (ICP) measurements, taken on a Perkin-Elmer Optima 4300DV inductively coupled plasma optical emission spectrometer (ICP-OES). The samples were dissolved in a 0.2% (v/v) solution of tetramethylammonium hydroxide, 0.05% Triton X-100 solution, and pumped at a rate of 1.5 mL/min. A solution of 10 ppm Y was added with an inline tee as an internal standard.

Temperature dependent EXAFS Cu (fluorescence) and Zn K-edge (transmission) data for the powdered ZnS:0.2%Cu NC sample were collected at the Stanford Synchrotron Radiation Laboratory (SSRL), beamline 10-2. Using a slit height of 0.5 mm, the energy resolution was approximately 1 eV. The NC powders were deposited on filter paper; one filter paper layer produced a Zn K-edge step height 0.3−0.5. The Si(111) monochromator was detuned 50% to reduce harmonics.

## 3. Results

**3.1. Optical Characterization: UV−Vis and PL.** The UV−vis absorption spectra of the crude product and the product after 2 h of reflux are shown in Figure 1. Prior to reflux, the ZnS:Cu,Cl sample shows a very narrow UV absorption excitonic peak at 292 nm, indicating a monodispersed size distribution of particles. After reflux, the peak is broadened and red-shifted to ~310 nm. This shift is due to particle growth, and the broadening is most likely due to a broader size distribution. Bulk ZnS absorbs at 340 nm, thus the particles exhibit a blue shift of 30 nm due to quantum confinement effects. The UV−vis spectra of ZnS, undoped or doped with copper, are indistinguishable, indicating that Cu-doping has no or little effect on the electronic absorption spectrum of ZnS.

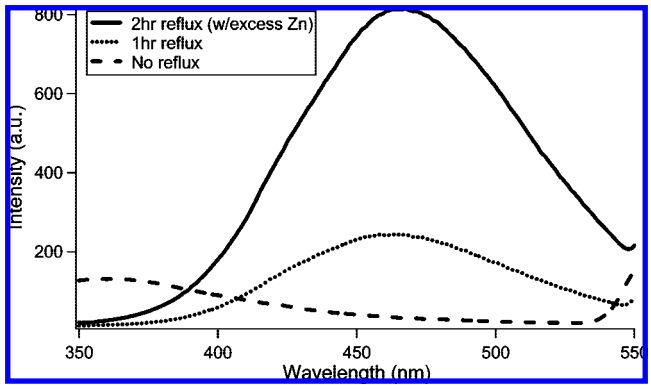


**Figure 2.** Photoluminescence (PL) spectra of ZnS:Cu,Cl crude product (dashed line), refluxed product (dotted line), and refluxed product after addition of excess Zn (solid line), $\lambda_{ex} = 280$ nm.

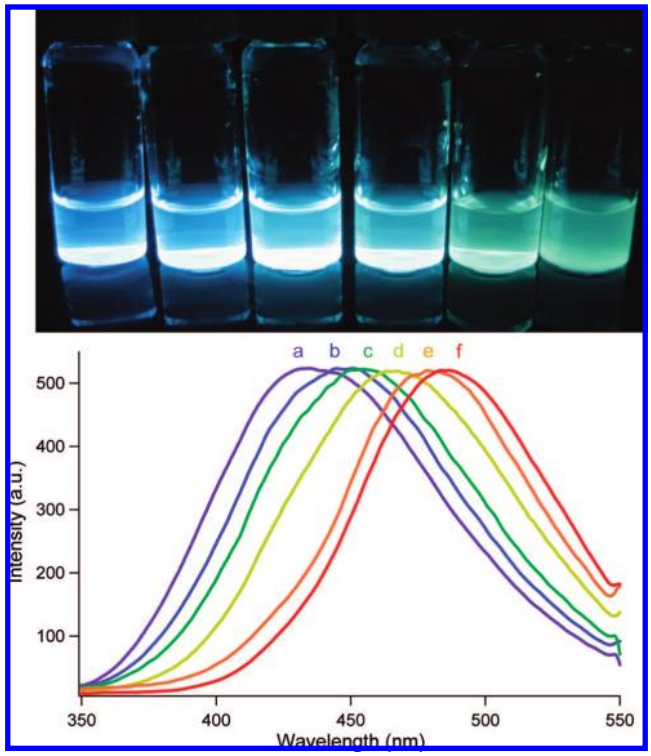


**Figure 3.** (Top) Photograph of ZnS NCs with different Cu dopant concentrations under UV-lamp irradiation, $\lambda_{ex} = 300$ nm, (a) 0%, (b) 0.2%, (c) 0.5%, (d) 1%, (e) 2%, and (f) 3% (from left to right). (Bottom) Normalized PL spectra of corresponding samples, $\lambda_{ex} = 280$ nm.

The crude product exhibits no PL at room temperature. Upon reflux of the ZnS:1%Cu NCs, a broad emission peak develops at 464 nm upon excitation at 280 nm (Figure 2). After 2 h of reflux and addition of excess Zn, the PL intensity increases by almost four times with a very slight shift in emission to 467 nm.

With addition of Cu to ZnS, the blue emission peak is red-shifted. The undoped NCs (with no Cu added) have an emission peak at ~440 nm. The emission peak may be pushed out as far as 487 nm (green emission) upon addition of 3% Cu. This is because the Cu green emission peak develops as the blue self-activated (SA) or Cu-complex trap state emission of ZnS becomes weaker. The normalized PL spectra of ZnS doped with copper concentrations of 0%, 0.2%, 0.5%, 1%, 2%, and 3% are shown in Figure 3. Clearly, the observed emission band is substantially red-shifted with addition of Cu. The corresponding samples under UV irradiation are displayed also. Addition of

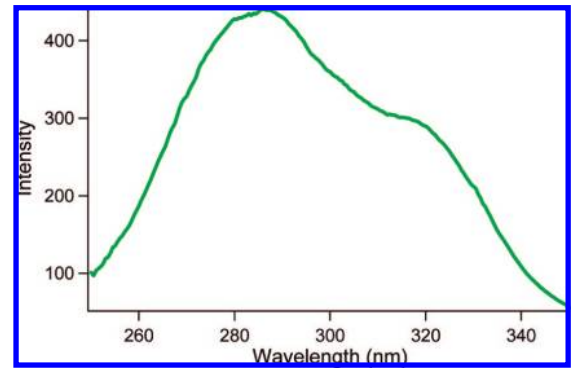


**Figure 4.** The photoluminescence excitation (PLE) spectrum of ZnS:1%Cu,Cl colloidal NCs for $\lambda_{em} = 465$ nm.

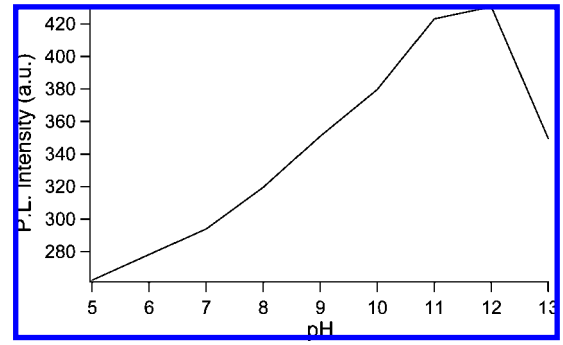


**Figure 5.** Change of PL intensity of ZnS:Cu,Cl colloidal NCs as a function of pH of the aqueous colloidal solution.

greater than 2% Cu led to only a vaguely detectable red-shift of the emission band in the PL spectra, as well as decreased stability of the sample. It took multiple attempts to synthesize particles with 2% and 3% copper doping. Upon completion, they aggregated to yield a cloudy solution within days of the synthesis. It seems that for best results in terms of stability and optical quality, no more than 1% Cu should be used.

Figure 4 shows one representative photoluminescence excitation (PLE) spectrum of ZnS:Cu,Cl with 1% Cu doping. The PLE spectrum essentially does not change with addition of Cu into ZnS, indicating that the excitation originates primarily from absorption of light by the ZnS host, as expected.

To gain a better understanding of the possible effect of surface characteristics, the PL was measured for ZnS:Cu,Cl colloidal NCs as a function of pH, since pH is known to affect the surface characteristics of aqueous colloidal nanocrystals.[54,55] Figure 5 shows the change of PL intensity for ZnS:Cu,Cl nanocrystals with 1% Cu doping as a function of different pH values. The PL clearly depends on pH with a noticeable increase in PL with increasing pH and a maximum PL at pH ~11−12. For this reason, the synthesis was carried out around pH 11. Below pH 5, the solution becomes cloudy and the NCs precipitate.

**3.2. Structural Characterization: XRD, ICP, and TEM.** The XRD patterns of the ZnS:Cu,Cl NCs, shown in Figure 6, reveal the cubic zinc blende structure of ZnS (JCPDS No. 05-0566). The broadness of the peaks is due to the small size of the crystals. The size of the particles, estimated using the Debye−Scherrer relation,[56] was ~3 nm.

ICP measurements confirmed Cu doping with an incorporation efficiency of almost unity, that is, all Cu ions added to the reaction were incorporated into the ZnS NCs. This seems to be a little higher than expected quantitatively. However, at a qualitative level, the ICP measurements are consistent with the observed PL attributed to Cu doping and the EXAFS data, to

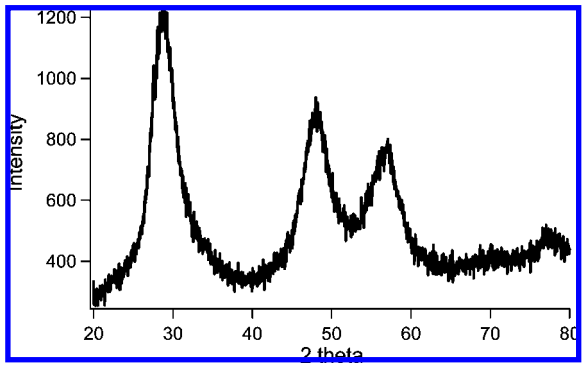


**Figure 6.** X-ray diffraction (XRD) pattern of ZnS:Cu,Cl NCs with 1% Cu doping.

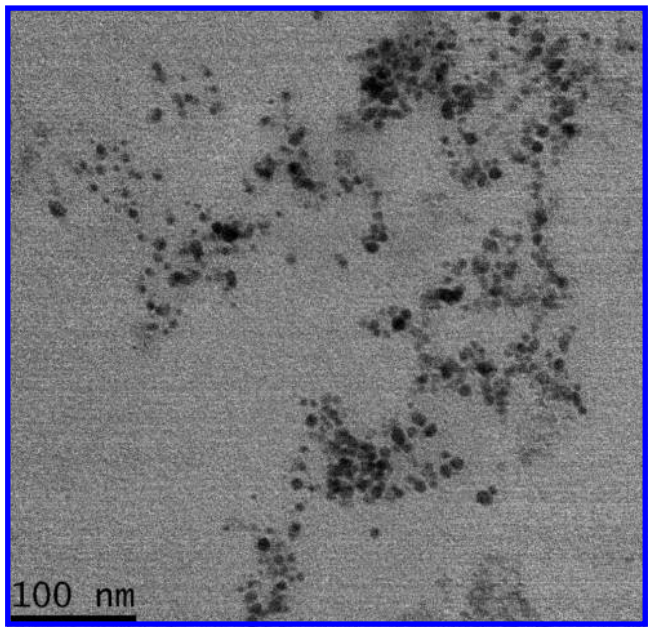


**Figure 7.** Transmission electron microscope (TEM) image of ZnS:Cu,Cl NCs with 1% doping.

be presented next, that indicate Cu is in a structure that has few second neighbors. The EXAFS data show that the nearest neighbor environment about Cu at low concentrations (0.2%) is very similar to that in CuS precipitates, as found in bulk doped material,[32] but there may be a larger fraction of Cu substitutional for Zn in the NCs. The ICP data are thus consistent with PL and EXAFS data in supporting a partial substitutional Cu doping in ZnS.

A representative TEM image of ZnS:Cu,Cl nanocrystals with 1% Cu doping is shown in Figure 7. The average size of the nanocrystals is approximately 6 nm. For other Cu doping levels and no doping, the average particle sizes are also similar.

**3.3. Structural Characterization: EXAFS.** To better understand the correlation between the optical properties and structural properties, EXAFS experiments have been carried out to determine the local structure about the ions in the ZnS:Cu,Cl NCs. A standard data reduction was used to extract the EXAFS oscillations in *k*-space; examples of the Zn K-edge and Cu K-edge *k*-space data for the ZnS:0.2%Cu NCs at 6 K are shown in Figure 8. The *k*-space data were then Fourier transformed into *r*-space (RSXAP package[57]). We use a *k*-space window of $k = 3.5-14$ Å$^{-1}$ for the Zn K-edge, with a Gaussian rounding of the FT window of width 0.3 Å$^{-1}$, while for the Cu K-edge, the FT range is $k = 3.5-11$ Å$^{-1}$, with the same Gaussian broadening.

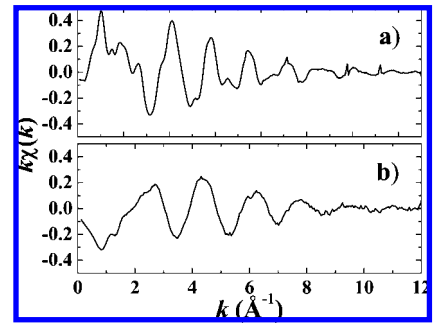


**Figure 8.** Plot of EXAFS *k*-space data for NC ZnS:0.2%Cu. (a) Zn K-edge data at $T = 6$ K, with a *k*-range of 0−15 Å$^{-1}$; (b) Cu K-edge data at $T = 6$ K, with a *k*-range of 0−12 Å$^{-1}$.

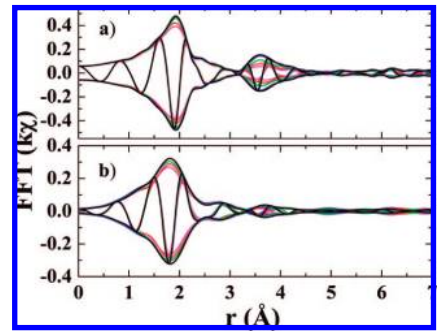


**Figure 9.** Plot of EXAFS r-space data for NC ZnS:0.2%Cu. (a) Zn K-edge, with *k*-range 3.5−14 Å$^{-1}$ and 0.3 Å$^{-1}$ Gaussian window broadening; (b) Cu K-edge, with *k*-range 3.5−11 Å$^{-1}$ and 0.3 Å$^{-1}$ Gaussian window broadening. $T = 6$ (black), 75 (blue), 150 (green), 225 (red), and 300 (purple) K.

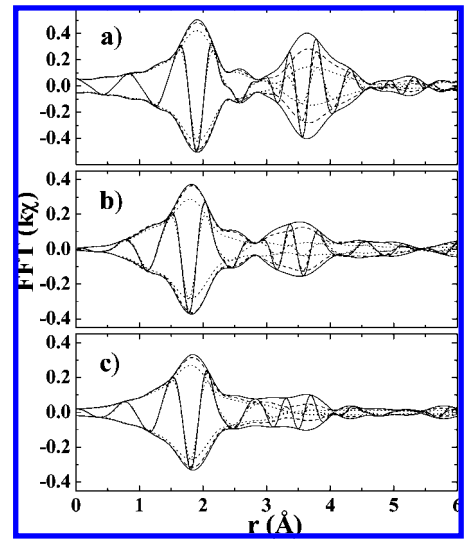


**Figure 10.** EXAFS *r*-space data for bulk material, at Cu and Zn K-edges. (a) Bulk ZnS:0.15%Cu,Cl, Zn K-edge, $T = 4$, 140, 300 K; (b) bulk ZnS:0.15%Cu,Cl, Cu K-edge, $T = 4$, 100, 300 K; and (c) bulk CuS reference, Cu K-edge, $T = 4$, 140, 300 K. Here the fast oscillation is the real part of the transform; *k*-range is 3.5−11 Å$^{-1}$ for Cu K-edge and 3.5−14 Å$^{-1}$ for Zn K-edge; window Gaussian broadened by 0.3 Å$^{-1}$.

Figure 9 shows plots of the Zn K-edge and Cu K-edge *r*-space data for the ZnS: 0.2%Cu NCs. To compare the NC results with commercial ZnS:Cu,Cl and pure CuS bulk samples, we plot in Figure 10 the Zn K-edge (top) and Cu K-edge (middle) *r*-space data for a bulk ZnS:Cu,Cl sample, as well as the Cu K-edge for a pure CuS sample.[58]

For the Zn K-edge, the difference between the first peak (Zn−S) is small in Figures 9a and 10a, but a large amplitude

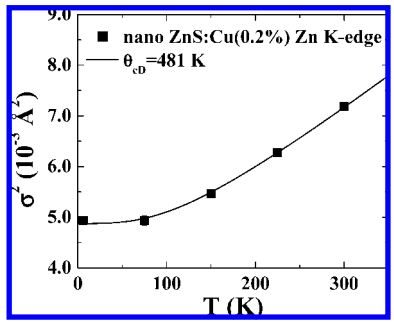


**Figure 11.** $\sigma^2(T)$ for Zn−S and the correlated Debye fit (solid line) for the ZnS:0.2%Cu,Cl NC sample (solid squares). The Zn K-edge data were fit over the range 1.3−2.2 Å. The correlated Debye temperature $\theta_{cD} = 481$ K is similar to the bulk sample's Zn K-edge result, 472 K. Errors in $\theta_{cD}$ are ±30 K.

difference is observed at the second peak (a combination of Zn−Zn and several weak multiple scattering peaks); the data for the NC sample clearly have a much smaller peak. It could be caused by the lack of Zn−Zn pairs (∼3.83 Å) due to the size effect for NCs or the presence of extra distortions in the Zn−Zn bonds near the NC surface. At the Cu K-edge, the first peak (Cu−S) is similar for nano ZnS:0.2%Cu and the bulk ZnS:Cu,Cl (see Figures 9b and 10b); however, the shoulder region (2−2.5 Å) looks more like the pure CuS reference for the bulk material, whereas it is smaller and more similar to the Zn data (i.e., a substitutional site) for the NCs. A much larger difference appears at the second peak; the amplitude for the NC is much smaller, and the shapes are quite different.

Next, the Zn K-edge data were fit to theoretical EXAFS functions for the zinc blende structure (generated by FEFF 8.20, developed by Rehr and co-workers[59]), using the program rsfit (RSXAP package);[57] the Cu K-edge data were fit similarly, but here we used both a pure CuS experimental standard, and FEFF functions for substitutional Cu in ZnS as described in more detail below. Our primary interest for the temperature ($T$)-dependent study is $\sigma(T)$, the width of the Zn−S or Cu−S pair distribution function (PDF), which parametrizes the amount of distortion present around the Zn or Cu ions.

The thermal phonon contributions were then determined from a fit of $\sigma^2(T)$ vs $T$, for $4 \leq T \leq 330$ K, to the correlated Debye model plus a static off-set. This model is usually a good approximation for all phonon modes including acoustic and optical phonons.[60]

In Figure 11 we show $\sigma^2(T)$ versus $T$ for Zn−S (Zn K-edge data) of the NC sample. The correlated Debye temperature ($\theta_{cD} = 481$ K) is identical (within errors ±30 K) to that for bulk ZnS:Cu,Cl ($\theta_{cD} = 479$ K), which shows identical Cu−S bond strengths.

To compare the further neighbors around Zn, we used a longer fit range (1.1−4.3 Å) and assumed a Gaussian PDF with a width $\sigma$ for each bond. The bond lengths were constrained to the ZnS cubic structure (only allowing small vibrations). For the bulk sample, we fixed the amplitude of each peak using $S_0^2 = 0.9$, to the coordination number N of the ZnS lattice, which is 4 for Zn−S at 2.34 Å and 12 for Zn−Zn at 3.83 Å. For the NC sample, all the constraints are the same as for the bulk, except for the amplitude of the Zn−Zn pair that is not constrained. Considering the nano-size of the ZnS lattice, a large fraction of Zn atoms are near the surface, which will reduce the averaged number of Zn−Zn pairs (3.83 Å) to less than 12.

The fits are both very good, and the results, such as bond length and local distortion, are similar in NC and bulk samples. As expected, the NC sample has a lower amplitude for the Zn−Zn pair, indicating a coordination number of ∼9−10, compared with the bulk, 12. This means that a significant fraction of the Zn atoms have less than 12 Zn neighbors at 3.83 Å. Since the NCs are almost spherically shaped, we varied the size of the ZnS particles and counted the number of Zn−Zn pairs (3.83 Å) versus NC diameter. The simulation shows the average NC has a diameter ∼3 nm. This size estimation is in good agreement with the Debye−Scherrer calculation of crystallite size of ∼3 nm. The size of the particles as characterized by TEM was bigger, closer to 6 nm. The reason for this discrepancy could be due to formation of a shell, possibly zinc hydroxide or zinc oxide, on the ZnS NCs. It could also be due to aggregation of the NCs, causing an aggregated cluster to appear as one large particle. Another possibility is the existence of multiple crystal domains, which were on average 3 nm in size.

Two earlier EXAFS studies of pure ZnS nanoparticles have been reported;[61,62] the nanoparticles studied appear to be uncapped in contrast to the NCs discussed here. Gilbert et al. found quite different values of $\sigma^2$ for their nanoparticles and bulk material while for our NC the values of $\sigma^2$ are comparable. Berlier et al. found that the Zn−Zn coordination number at low $T$ is quite low, 4−5 instead of 12, whereas we find the coordination number to be 9−10. We suggest that the main difference is that the capping allows the surface to relax toward the bulk structure and the surface is less distorted.

For the Cu K-edge data, we first fit the NC ZnS:0.2%Cu,Cl and bulk ZnS:0.15%Cu,Cl samples using a pure experimental CuS standard and found some small differences. First, the nearest neighbor Cu−S peak height is slightly larger in the NC sample than in bulk; second, to fit the data, the average Cu−S bond length for the NC sample is very slightly shorter, ∼0.01 Å, but it is within the range of our experimental errors. Thus within 0.01 Å, the position of the first Cu−S peak is at the same position for the Cu-doped NC, the bulk Cu-doped samples, and the CuS material; note the average Cu−S distance in the CuS structure is ∼2.27 Å.

If instead we fit the Cu K-edge data (doped bulk and NC samples) with a Cu−S theoretical function calculated using FEFF[63] for a zinc-blende structure, then the NC sample has a comparable low value of the $S_0^2$ parameter but slightly less disorder for the Cu−S peak compared to the doped bulk sample. In both cases the Cu−S peak is contracted by 0.07−08 Å compared to the Zn−S bond distance of 2.34; that is, the average distance is again 2.26−2.27 Å.

Unfortunately, we do not know the Cu−S bond length for isolated substitutional Cu in ZnS. Because CuS precipitates form at low Cu concentrations, it would likely require Cu concentrations as low as 100 ppm to eliminate such precipitates. However, the ionic radii for $Cu^{1+}$ and $Zn^{2+}$ are very similar (∼0.074 nm), and the Cu−Cl bond length in CuCl is identical to the Zn−S bond length in ZnS. Consequently one might expect that for substitutional $Cu^{1+}$ in ZnS, the Cu−S bond length would be similar to that of Zn−S. Since the average Cu−S bond length in the doped samples is very close to that in CuS and significantly shorter than the Zn−S bond length, it is likely that a significant fraction of the Cu is in very small CuS-like precipitates. Not all the Cu is in CuS, however, because the PL shows a clear red-shift with increasing Cu concentration, indicating Cu-doping inside ZnS, and the amplitude of the high-$r$ part of the Cu−S EXAFS peak (2−2.5 Å, see Figures 9 and 10) in NC ZnS:Cu,Cl is lower than bulk ZnS:Cu,Cl or CuS. Thus it appears that in the NC ZnS:0.2%Cu,Cl, most of the Cu is also in CuS-like clusters (precipitates) but with a slightly

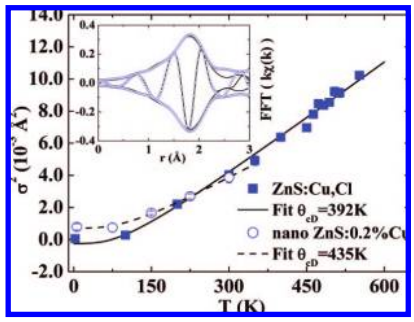


**Figure 12.** $\sigma^2$ vs $T$ for Cu K-edge data and their correlated Debye fit: for nano ZnS:Cu(0.2%),Cl sample (open circles), the correlated Debye fit (dashed black line) gives a Debye temperature of 435 K; for bulk ZnS:Cu,Cl sample (solid squares),[58] the Debye fit (solid line) gives a Debye temperature of 392 K. Inset is a fit (open circles) to the nearest Cu−S bond for the NC sample data (solid line). Fit range is 1.3−2.2 Å. The error bar is comparable to the size of the symbols.

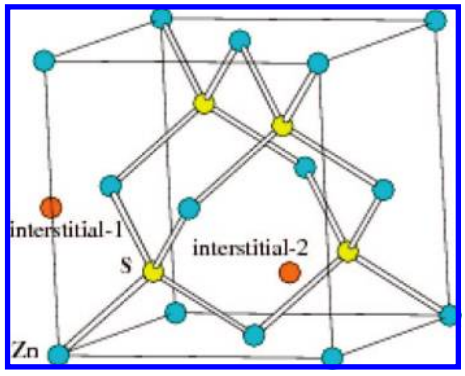


**Figure 13.** A cubic unit cell of zinc blende, illustrating the two interstitial sites for Cu (orange). Blue and yellow are for Zn and S, respectively.

larger fraction of substitutional Cu in the ZnS host compared to the doped bulk samples ZnS:0.15%Cu,Cl.

In Figure 12, we compared $\sigma^2(T)$ for bulk and NC samples for the nearest Cu−S pairs (Cu K-edge) and also plot fits to the correlated Debye model. Though $\sigma^2(T)$ for the NC ZnS: 0.2% Cu data has a slightly larger static distortion than other bulk samples, the $T$-dependence gives a slightly larger Debye temperature (435 K) to that for the bulk ZnS:Cu,Cl (392 K), comparable to the CuS reference sample (430 K); however, a 10% variation is within the systematic error of these correlated Debye fits. This implies that the Cu atoms in the NC sample have a similar nearest neighbor local environment/structure and comparable Cu−S bond strength to bulk ZnS:Cu,Cl samples. Surprisingly, the second neighbor Cu−Zn/Cu peak is not well defined—much less so than for the Zn K-edge peak in the same sample. This suggests that, for the Cu-doped NCs, most of the Cu atoms are near the surface.

We note that there are two possible interstitial sites for Cu atoms. As shown in Figure 13, the first interstitial Cu site (interstitial 1 in Figure 13) has four S nearest neighbors at the distance of 2.34 Å and six Zn atoms at the distance of 2.70 Å, while the second interstitial Cu site (interstitial 2) has four Zn nearest neighbors at 2.34 Å and six S at 2.70 Å. We used these structures to calculate theoretical Cu−S and Cu−Zn FEFF functions and fit the data over the range of 1.3 ∼ 2.5 Å. For the first interstitial Cu site, the only constraint we put into the fit is to fix the amplitude of the Cu−S function, while we let the amplitude of the Cu−Zn function vary to see how much Cu−Zn is needed at this short distance. The fit result showed a shift of the Cu−S by −0.07 Å (as observed for the bulk samples), and the amplitude of the Cu−Zn peak drops to almost zero. This implies that the first Cu interstitial site likely does not exist in the NCs. A similar fit was done with a fraction of the Cu on the second interstitial Cu site and again led to the same result—no Cu on this interstitial site. However, due to the amplitude uncertainty in EXAFS, we cannot completely eliminate the possibility of some interstitial $Cu^+$, but the fraction would have to be much smaller than 5%. Since a sizable fraction of Cu is in a CuS-like precipitate we cannot place a better constraint on the presence of $Cu^+$.

We also fit the NC data to a Cu substitutional site, in which the Cu replace Zn in the ZnS NCs. In this case the substitutional Cu has only four S nearest neighbors at 2.34 Å. The fit showed comparable fit quality with the experimental standard fit, with the distance contracted by 0.08 Å as above, and the correlated Debye temperature about the same within error. However, the amplitude reduction parameter $S_0^2$ (0.68) is somewhat smaller than expected (∼0.75) and again indicates a significant fraction of Cu is in CuS precipitates.

## 4. Discussion

**4.1. Oxidation State of Copper.** Even with the long history and many studies on ZnS:Cu,Cl several issues concerning this system are still subjects of active ongoing research and discussion, including the mechanism of doping, the oxidation state of the dopant, and the electronic energy levels of the dopant involved relative to the band edge of the ZnS host. There are a number of explanations proposed in the literature that are sometimes inconsistent.

For example, one of the most basic issues is the oxidation state of the copper dopant. Several recent reports suggested that the copper ion exists as $Cu^{2+}$.[64−66] This is, however, in contradiction with early magnetic susceptibility measurements that showed that the dopant exists as $Cu^+$.[50] These measurements show that ZnS, pure or doped with Cu and Cl, is diamagnetic, and hence there are no unpaired spins. Since the electron configuration of $Cu^+$ is $d^{10}$, only this form would be diamagnetic. If copper existed as $Cu^0$ or $Cu^{2+}$ in the ZnS, the system would be strongly paramagnetic. The susceptibility experiments revealed that for very low concentrations of Cu, up to high concentrations in which aggregates of CuS would form, the system always remained diamagnetic. The oxidation state of Cu in CuS is also +1.[67] This is consistent with electron paramagnetic resonance (EPR) experiments that found ZnS:Cu,Cl to be diamagnetic, except under excitation when it became paramagnetic.[68] Under optical excitation, an electron from the valence band of ZnS is excited to the conduction band. The hole in the valence band now accepts an electron from $Cu^+$ with a $d^{10}$ electron configuration, leaving $Cu^{2+}$ with a $d^9$ configuration. This excited electronic configuration is now paramagnetic.

In multiple low and high temperature EPR measurements that were performed on our Cu-doped ZnS NCs, with varying concentrations of copper and no optical excitation, no Cu signal was ever detected. The source of copper used in the experiments was $CuCl_2$, which is $Cu^{2+}$. We believe that $S^{2-}$ acts as a reducing agent to convert the $Cu^{2+}$ to $Cu^+$. The reduction potential of the reaction

$$2Cu^{2+} + S^{2-} \rightarrow 2Cu^{+} + S \qquad (1)$$

is 0.606 V vs SHE. One mechanism that could apply to our system has been proposed for the incorporation of $Cu^+$ into CdS nanoparticles from its $Cu^{2+}$ precursor.[69] This mechanism involves the transfer of an electron from a sulfur vacancy to

the $Cu^{2+}$ to reduce it to $Cu^{+}$. Though we did not do mechanistic studies to determine the exact manner in which the Cu is reduced, our EPR studies, paired with past observations of ZnS:Cu systems, imply that the oxidation state of Cu in our system is +1.

**4.2. Photoluminescence and Associated Energy Levels.** ***4.2.1. Undoped ZnS.*** To understand the energy levels of the doped and undoped nanocrystalline ZnS, it is useful to look back on what is known about the properties of the corresponding bulk system. Pure bulk ZnS crystals exhibit emission in the ultraviolet region, but none in the visible.[70] In an imperfect crystal, blue emission is observed, which is often referred to as the self-activated (SA) emission peak of ZnS. There are three key models which have been proposed to describe this emission: the Lambe−Klick model that involves emission from a donor to the valence band of ZnS,[71] the Klasens−Schön model that is the emission from the conduction band to an acceptor,[72,73] and the Williams−Prener model, proposing an inter-bandgap transition between a two-level associated donor−acceptor (D−A) pair.[74] Though support in the literature has been shown for all three of these models, the most convincing studies support the Williams−Prener model.[75−78] Shionoya's group has used polarization experiments to show that the symmetry of the SA center must be $C_{3v}$, and the only way this is possible is by having an associated center.[77]

The next question that follows naturally is the identity of the SA centers. Since the peak is absent in the perfect crystal and becomes very strong with addition of a coactivator ($Cl^{-}$, $Al^{3+}$, or a variety of others), the impurity must be part of the luminescent mechanism. For charge compensation, a zinc vacancy would accompany incorporation of two $Cl^{-}$ ions substituting on two S sites or two $Al^{3+}$ substituting for two $Zn^{2+}$. By the symmetry of the center,[77] one of these substitutional $Cl^{-}$ atoms would associate with a $Zn^{2+}$ vacancy at the nearest neighbor site, while the other would instead be isolated in the crystal and responsible for the initial state of the emission. The isolated coactivator would be an electron trap near the bottom of the ZnS conduction band, while the complex involving the zinc vacancy and a neighboring coactivator would be a hole trap above the top of the ZnS valence band. The energy level diagram is schematically shown in Figure 14.

The mechanism for the emission begins with excitation of an electron from the valence band (VB) to the conduction band (CB) in the host ZnS. Next, the complex, involving a tetrahedral $Zn^{2+}$ vacancy surrounded by three $S^{2-}$ and a $Cl^{-}$, will donate an electron into the hole left in the valence band, leaving a hole in the hole trap state. The excited electron in the conduction band will fall into a shallow electron trap state associated with $Cl^{-}$ or other impurities, from where it will combine with the hole located on the $Zn^{2+}$ vacancy complex or hole trap state. A photon, ~440 nm (2.8 eV), is emitted during the trapped electron−hole recombination. Peak broadening is due to the varied local environment of the defects, which leads to slight decreases or increases in energy.

This is the mechanism developed for the SA emission of bulk ZnS, which we believe could apply also to our undoped NCs. In our experiments, we did not intentionally add any impurities to the system. However, even if an effort is made to keep the system completely clean, it is very difficult to prevent inclusion of a small amount of impurity. The sodium hydroxide used in the synthesis was only 98.5% pure, and both Al and Cl were listed as impurities in the trace analysis. It is also known that many NC systems can have significant concentrations of Schottky and Frenkel defects, which for ZnS are Zn and S vacancies and Zn and S interstitial atoms, respectively.[79−81] Schottky defects are more prevalent in cubic zinc blende, and only Zn Frenkel defects are formed.[82,83] These defects may also be responsible for contributing trap-states that lead to the SA emission.

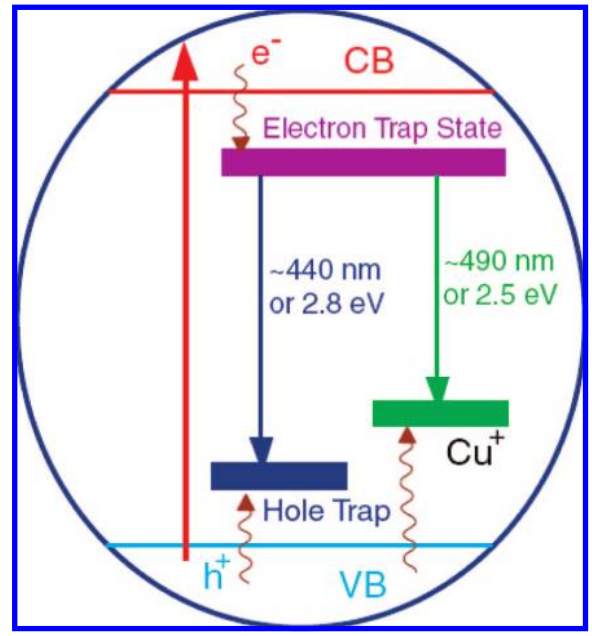


**Figure 14.** Proposed energy diagram for Cu doped and undoped ZnS NCs. The blue SA emission at 440 nm (2.8 eV) and green Cu emission at 490 nm (2.5 eV) transitions are illustrated as originated from impurity-induced shallow trap states near the bottom of the conduction band of ZnS. The hole trap is attributed to a combination of a zinc vacancy plus three $S^{2-}$ and one $Cl^{-}$ on the nearest neighbor (S) sites; a second isolated $Cl^{-}$ or other impurity ion, which is needed for charge compensation and is located a few lattice sites away, is proposed to be responsible for the an electron trap. The electron trap states are 0.1−0.3 eV below the CB, and the hole acceptor states are just approximately 0.6−0.8 eV above the top of the VB.

It has also been observed in the literature that in a NC sample with an increasing S:Zn ratio, the SA emission decreases. This has been attributed to fewer sulfur vacancies and thus fewer emissive centers with increasing S:Zn ratio.[64,84,85] This observation of decreased luminescence alone is difficult to attribute to fewer S vacancies because of the important role of surface chemistry in the luminescent behavior of the NCs (see discussion below). Since excess $S^{2-}$ could quench the luminescence by adding surface states that lead to nonradiative recombination, its excess cannot be attributed to eliminating vacancies that would have led to luminescence.

***4.2.2. ZnS Doped with Cu and Cl.*** Bulk ZnS doped with copper is known to have three PL emission bands: blue, green, and red.[50,51] Polarization experiments done by Urabe and Suzuki showed that the blue and red copper luminescent centers have lower symmetry than the host lattice, indicating that they must be associated centers.[86,87] The green peak was found to not have lower symmetry than the lattice and, hence, not be spatially associated with the coactivator.[88] Previous work has shown that the appearance of the three peaks is dependent on the ratio of activator to coactivator ($Cu^{+}$/$Cl^{-}$ in our system).[89,90] The blue peak is present when the concentration of $Cu^{+}$ is greater than the concentration of $Cl^{-}$; the red peak when there is a much greater concentration of $Cu^{+}$ than $Cl^{-}$ or no $Cl^{-}$; and last the green peak when there is a roughly equal ratio of $Cu^{+}$ to $Cl^{-}$ present.

The model proposed for the Cu-blue peak suggests spatial association of an interstitial $Cu^+$ with a substitutional $Cu^+$.[91] This type of $Cu^+$ association was demonstrated in ZnSe[92] and is said to be responsible for its green emission peak, which corresponds to the blue emission peak in ZnS. In the 2% and 3% Cu doped PL spectra of the NCs, shown in Figure 3, a blue shoulder is observed that could potentially be due to the Cu blue peak. It resembles the shoulder present in Bower's PL emission spectrum of ZnS:Cu,Cl at room temperature, which is considerably enhanced at 77 K.[50] In the present system, since this peak is located at the exact same position as the blue SA peak that is present before Cu dopant is added, we cannot conclusively assign this peak to be resultant from Cu.

In addition to the lack of definitive optical data to confirm the presence of this transition, the EXAFS data also do not provide evidence about this center. If this $Cu^+$ pair center were present, it would require a significant fraction of interstitial $Cu^+$ which would have a clear signal in our EXAFS data. This scenario was modeled and did not fit our data, as described above. This places an upper limit that at most a few percent of Cu is interstitial $Cu^+$. However, since we cannot determine the relative fractions of Cu in CuS precipitate and as substitutional Cu, as described above, we cannot definitively say there are no $Cu^+$ pair centers. It would require EXAFS data on extremely dilute samples (100 ppm) to clarify this issue.

The red Cu center has been attributed to the spatial association of a substitutional $Cu^+$ with a $S^{2-}$ vacancy in nearest-neighbor sites. This peak is most often observed in Cu doped samples, without a coactivator.[50] It was not observed in any of our samples. Though our PL spectra do not show emission past 550 nm, this further region was scanned and no peaks were found.

The green $Cu^+$ center is formed in the presence of an equal amount of $Cu^+$ with its coactivator ($Cl^-$, $Al^{3+}$, or $Br^-$). The activator and coactivator are randomly distributed throughout the crystal, occupying substitutional sites in the lattice, but are not spatially associated. Together they form a donor−acceptor (D−A) pair. This green $Cu^+$ center was observed in our samples, evidenced by the increasingly red-shifted emission (from blue to green) with increasing concentration of copper, as shown in Figure 3. Since the green Cu center is due to transitions between $Cl^-$ and $Cu^+$ levels, this is a good indication that comparable concentrations of the two dopants are present. If very different concentrations of $Cl^-$ and $Cu^+$ were present in the particles, either blue or red emission would be observed.

**4.3. Surface Effect on Photoluminescence.** The addition of excess zinc, after the initial formation of the NCs, serves to stabilize the particles as well as increase their fluorescence. This phenomenon has been observed in a number of different systems.[93−95] The mercapto end of MPA is expected to bind to the $Zn^{2+}$ on the NC surface. Therefore, sulfide groups on the surface are unpassivated by the capping ligand and create dangling bonds, which may act as nonradiative combination centers. Alternatively, the high pH of the solution enables formation of a zinc hydroxide layer around the ZnS NCs. Upon addition of excess zinc, the sulfide dangling bonds are passivated and allow a more complete coverage of the NC with either the capping molecule or the zinc hydroxide. This coverage creates much more stable particles, allowing the NCs to remain dispersed in water for months. Without excess zinc, the solution becomes cloudy and loses its fluorescence within days. The excess zinc also increases the PL of the NCs for the same reason. Since the capping shell is more complete with less dangling sulfide bonds, surface trap states that allow nonradiative relaxation pathways are reduced. This can be observed in Figure 2, where particles exhibit PL intensity four times greater after the addition of excess zinc into the reaction mix.

Addition of too much excess zinc (more than 4× Zn:S) causes flocculation of the particles and loss of luminescent properties. This effect is attributed to the $Zn^{2+}$ removing the effective negative charge of the NCs' surface. The capping molecule, MPA, has a carboxylic acid headgroup that is deprotonated under the high pH reaction conditions. This causes the NCs to have a negatively charged surface, which makes them soluble in water and repelled from one another in solution enough to prevent aggregation. When a large excess of $Zn^{2+}$ is introduced, the negatively charged surface is shielded by the $Zn^{2+}$ and becomes effectively neutral. This causes aggregation and flocculation of the particles.

The effect of the pH on the NCs' PL properties, shown in Figure 5, can also be explained via surface charge and interactions. At pH < 5, the particles precipitate out of solution, so fluorescence data could not be gathered. This can be explained by the $pK_a$ of MPA, which is 4.3.[96] Below this pH, the carboxylic acid head groups are protonated and thus neutral. The change in the surface charge going from negatively charged to neutral causes the interaction of the NCs with water to become unfavorable, and they lose their solubility, while the interaction with each other becomes more favorable and aggregation may occur. The stronger PL at higher pH is consistent with previous studies of similar NCs such as CdS.[54,97,98] The explanation was that surface trap states due to species like $HS^-$ were converted into $HO^-$ at higher pH, resulting in better surface passivation and thereby increased PL. The same explanation could apply to the current ZnS NCs. Direct confirmation of this hypothesis, however, has been challenging and will need to be investigated in the future.

## 5. Conclusion

Stable, fluorescent ZnS:Cu,Cl NCs were synthesized with varying concentrations of $Cu^+$. The nanoscale dimensions of the system were confirmed by the blue-shifted excitonic absorption peak from that of bulk ZnS as well as XRD and TEM data. Cu-doping was confirmed by a red-shift in PL emission wavelength while ICP directly measured the amount of copper. The optical emission is proposed to arise from trapped electron−hole recombination within the ZnS bandgap. The Zn−S local structure in the NCs, as revealed by EXAFS, was comparable to that of bulk ZnS. However, the further neighbor peaks were less pronounced than those in the bulk, due to the nanodimensions of the crystals; the Zn−Zn peak had about 9−10 neighbors indicating a NC size ∼3 nm.

The location of much of the $Cu^+$ in the ZnS NC at 0.2% Cu is consistent with Cu in tiny CuS precipitates with an average bond length of 2.26−2.27 Å, possibly on the surface because the further neighbor peaks are so small for the NCs. There must still be a fraction of substituted sites to observe the shift in PL, but the fraction cannot be easily determined. Studies of the changes in the broadening of the Cu−S peak with temperature show that the strength of the Cu−S bond is comparable in Cu-doped bulk and NC ZnS and also similar to the Cu−S bond strength in bulk Cu−S; the correlated Debye temperatures are all near 400 K. Finally, we considered the possibility of a small fraction of Cu on interstitial sites which would have large Cu−Zn peaks at short pair distances. The fits pushed the concentration of such short Cu−Zn peaks to ∼0; at most a few percent of the Cu could be interstitial $Cu^+$.

This study represents the first attempt to use EXAFS to study the local structure about dopant atoms or ions in ZnS:Cu,Cl

NCs, to examine their unique structures on the nanoscale as compared to bulk, as well as to determine their correlation with optical properties with emphasis on PL that is important for exploiting potential applications of such materials in electroluminescence and other optical devices applications.

**Acknowledgment.** This project is funded by the U.S. Department of Energy (DE-FG02-07ER46388-A002). We would also like to thank the NSF Summer Undergraduate Research Fellowship (SURF) program for supporting Fadekemi Oba. We thank Abe Wolcott for helpful discussions.

## References and Notes

(1) Efros, A. L.; Efros, A. L. *Fizika i Tekhnika Poluprovodnikov* **1982**, *16*, 1209.
(2) Brus, L. E. *J. Phys. Chem.* **1983**, *79*, 5566.
(3) Nirmal, M.; Dabbousi, B. O.; Bawendi, M. G.; Macklin, J. J.; Trautman, J. K.; Harris, T. D.; Brus, L. E. *Nature* **1996**, *383*, 802.
(4) Chen, C. C.; Herhold, A. B.; Johnson, C. S.; Alivisatos, A. P. *Science* **1997**, *276*, 398.
(5) Chan, W. C. W.; Nie, S. M. *Science* **1998**, *281*, 2016.
(6) Murray, C. B.; Kagan, C. R.; Bawendi, M. G. *Annu. Rev. Mater. Sci.* **2000**, *30*, 545.
(7) Rogach, A. L.; Nagesha, D.; Ostrander, J. W.; Giersig, M.; Kotov, N. A. *Chem. Mater.* **2000**, *12*, 2676.
(8) Zhang, J. Z. *J. Phys. Chem. B* **2000**, *104*, 7239.
(9) Shim, M.; Wang, C. J.; Guyot-Sionnest, P. *J. Phys. Chem. B* **2001**, *105*, 2369.
(10) Peng, X. G. *Adv. Mater.* **2003**, *15*, 459.
(11) Burda, C.; Chen, X. B.; Narayanan, R.; El-Sayed, M. A. *Chem. Rev.* **2005**, *105*, 1025.
(12) Blackman, B.; Battaglia, D. M.; Mishima, T. D.; Johnson, M. B.; Peng, X. G. *Chem. Mater.* **2007**, *19*, 3815.
(13) Klimov, V. I.; Ivanov, S. A.; Nanda, J.; Achermann, M.; Bezel, I.; McGuire, J. A.; Piryatinski, A. *Nature* **2007**, *447*, 441.
(14) Deng, M. C.; Chin, T. S.; Chen, F. R. *J. Appl. Phys.* **1994**, *75*, 5888.
(15) Chamarro, M. A.; Voliotis, V.; Grousson, R.; Lavallard, P.; Gacoin, T.; Counio, G.; Boilot, J. P.; Cases, R. *J. Cryst. Growth* **1996**, *159*, 853.
(16) Smith, B. A.; Zhang, J. Z.; Joly, A.; Liu, J. *Phys. Rev. B* **2000**, *62*, 2021.
(17) Yang, H. S.; Holloway, P. H.; Ratna, B. B. *J. Appl. Phys.* **2003**, *93*, 586.
(18) Lu, W. G.; Gao, P. X.; Bin Jian, W.; Wang, Z. L.; Fang, J. Y. *J. Am. Chem. Soc.* **2004**, *126*, 14816.
(19) Viswanatha, R.; Sapra, S.; Sen Gupta, S.; Satpati, B.; Satyam, P. V.; Dev, B. N.; Sarma, D. D. *J. Phys. Chem. B* **2004**, *108*, 6303.
(20) Chen, W.; Zhang, J. Z.; Joly, A. *J. Nanosci. Nanotechnol.* **2004**, *4*, 919.
(21) Ghosh, M.; Seshadri, R.; Rao, C. N. R. *J. Nanosci. Nanotechnol.* **2004**, *4*, 136.
(22) Norberg, N. S.; Parks, G. L.; Salley, G. M.; Gamelin, D. R. *J. Am. Chem. Soc.* **2006**, *128*, 13195.
(23) Pradhan, N.; Battaglia, D. M.; Liu, Y. C.; Peng, X. G. *Nano Lett.* **2007**, *7*, 312.
(24) Janssen, N.; Whitaker, K. M.; Gamelin, D. R.; Bratschitsch, R. *Nano Lett.* **2008**, *8*, 1991.
(25) Beaulac, R.; Archer, P. I.; Gamelin, D. R. *J. Solid State Chem.* **2008**, *181*, 1582.
(26) Revathi, R.; Kutty, T. R. N. *J. Mater. Sci.* **1986**, *21*, 2100.
(27) Huang, J. M.; Yang, Y.; Xue, S. H.; Yang, B.; Liu, S. Y.; Shen, J. C. *Appl. Phys. Lett.* **1997**, *70*, 2335.
(28) Tanaka, S.; Kobayashi, H.; Sasakura, H. Electroluminescence materials. In *Phosphor Handbook*; Shionoya, S., Yen, W. M., Eds.; CRC Press: New York, 1999; p 601.
(29) Liu, H. W.; Laskar, I. R.; Huang, C. P.; Cheng, J. A.; Cheng, S. S.; Luo, L. Y.; Wang, H. R.; Chen, T. M. *Thin Solid Films* **2005**, *489*, 296.
(30) Manzoor, K.; Aditya, V.; Vadera, S. R.; Kumar, N.; Kutty, T. R. N. *Solid State Commun.* **2005**, *135*, 16.
(31) Xuan, Y.; Pan, D. C.; Zhao, N.; Ji, X. L.; Ma, D. G. *Nanotechnology* **2006**, *17*, 4966.
(32) Warkentin, M.; Bridges, F.; Carter, S. A.; Anderson, M. *Phys. Rev. B* **2007**, *75*, 075301.
(33) Yang, Y.; Huang, J. M.; Liu, S. Y.; Shen, J. C. *J. Mater. Chem.* **1997**, *7*, 131.
(34) Leeb, J.; Gebhardt, V.; Muller, G.; Haarer, D.; Su, D.; Giersig, M.; McMahon, G.; Spanhel, L. *J. Phys. Chem. B* **1999**, *103*, 7839.
(35) Toyama, T.; Adachi, D.; Fujii, M.; Nakano, Y.; Okamoto, H. *J. Non-Cryst. Solids* **2002**, *299*, 1111.
(36) Zhao, J. L.; Zhang, J. Y.; Jiang, C. Y.; Bohnenberger, J.; Basche, T.; Mews, A. *J. Appl. Phys.* **2004**, *96*, 3206.
(37) Morozova, N. K.; Galstyan, V. G.; Muratova, V. I.; Veselkova, M. M.; Pashenko, Y. A. *Inorg. Mater.* **1985**, *21*, 1433.
(38) Soo, Y. L.; Ming, Z. H.; Huang, S. W.; Kao, Y. H.; Bhargava, R. N.; Gallagher, D. *Phys. Rev. B: Condens. Matter* **1994**, *50*, 7602.
(39) Jin, C. M.; Yu, J. Q.; Sun, L. D.; Dou, K.; Hou, S. G.; Zhao, J. L.; Chen, Y. M.; Huang, S. H. *J. Lumin.* **1995**, *66−7*, 315.
(40) Dinsmore, A. D.; Hsu, D. S.; Gray, H. F.; Qadri, S. B.; Tian, Y.; Ratna, B. R. *Appl. Phys. Lett.* **1999**, *75*, 802.
(41) Kishimoto, S.; Hasegawa, T.; Kinto, H.; Matsumoto, O.; Iida, S. *J. Cryst. Growth* **2000**, *214*, 556.
(42) Ollinger, M.; Craciun, V.; Singh, R. K. *Appl. Phys. Lett.* **2002**, *80*, 1927.
(43) Tsujii, N.; Kitazawa, H.; Kido, G. *J. Appl. Phys.* **2003**, *93*, 6957.
(44) Li, G. H.; Su, F. H.; Ma, B. S.; Ding, K.; Xu, S. J.; Chen, W. *Phys. Status Solidi B* **2004**, *241*, 3248.
(45) Korotchenkov, O. A.; Cantarero, A.; Shpak, A. P.; Kunitskii, Y. A.; Senkevich, A. I.; Borovoy, M. O.; Nadtochii, A. B. *Nanotechnology* **2005**, *16*, 2033.
(46) Warad, H. C.; Ghosh, S. C.; Hemtanon, B.; Thanachayanont, C.; Dutta, J. *Sci. Techn. Adv. Mater.* **2005**, *6*, 296.
(47) Borse, P. H.; Vogel, W.; Kulkarni, S. K. *J. Colloid Interface Sci.* **2006**, *293*, 437.
(48) Arai, T.; Senda, S. I.; Sato, Y.; Takahashi, H.; Shinoda, K.; Jeyadevan, B.; Tohji, K. *Chem. Mater.* **2008**, *20*, 1997.
(49) Fischer, A. G. *J. Electrochem. Soc.* **1963**, *110*, 733.
(50) Bowers, R.; Melamed, N. T. *Phys. Rev.* **1955**, *99*, 1781.
(51) Shionoya, S., Yen, W. M., Eds. *Phosphor Handbook*; CRC Press: New York, 1999.
(52) Norman, T. J.; Magana, D.; Wilson, T.; Burns, C.; Zhang, J. Z.; Cao, D.; Bridges, F. *J. Phys. Chem. B* **2003**, *107*, 6309.
(53) Zhuang, J.; Zhang, X.; Wang, G.; Li, D.; Yang, W.; Li, T. *J. Mater. Chem.* **2003**, *13*, 1853.
(54) Wu, F.; Zhang, J. Z.; Kho, R.; Mehra, R. K. *Chem. Phys. Lett.* **2000**, *330*, 237.
(55) Li, H.; Shih, W. Y.; Shih, W. *Nanotechnology* **2007**, *18*, 495605.
(56) Ghosh, G.; Naskar, M. K.; Patra, A.; Chatterjee, M. *Opt. Mater.* **2006**, *28*, 1047.
(57) Booth, C. H. *R-Space X-ray Absorption Package*, 2005.
(58) Stanley, J.; Jiang, Y.; Bridges, F.; Carter, S. A. **2008**, in preparation.
(59) Ankudinov, A. L.; Ravel, B.; Rehr, J. J.; Conradson, S. D. *Phys. Rev. B* **1998**, *58*, 7565.
(60) Ashcroft, N. W.; Mermin, N. D. *Solid State Physics*; Saunders College: Philadelphia, 1976.
(61) Berlier, G.; Meneau, F.; Sankar, G.; Catlow, C. R. A.; Thomas, J. M.; Spliethoff, B.; Schuth, F.; Coluccia, S. *Res. Chem. Intermed.* **2006**, *32*, 683.
(62) Gilbert, B.; Huang, F.; Zhang, H.; Waychunas, G. A.; Banfield, J. F. *Science* **2004**, *305*, 651.
(63) Zabinsky, S. I.; Rehr, J. J.; Ankudinov, A.; Albers, R. C.; Eller, M. J. *Phys. Rev. B* **1995**, *52*, 2995.
(64) Bol, A. A. *J. Lumin.* **2002**, *99*, 325.
(65) Wang, M.; Sun, L.; Fu, X.; Liao, C.; Yan, C. *Solid State Commun.* **2000**, *115*, 493.
(66) Yang, P.; Lu, M.; Xu, D.; Yuan, D.; Song, C. *J. Phys. Chem. Solids* **2003**, *64*, 155.
(67) Luther, G. W., III; Theberge, S. M.; Rozan, T. F.; Rickard, D.; Rowlands, C. C.; Oldroyd, A. *Environ. Sci. Technol.* **2002**, *36*, 394.
(68) Holton, W. C.; De Wit, M.; Watts, R. K.; Estle, T. L.; Schneider, J. *J. Phys. Chem. Solids* **1969**, *30*, 963.
(69) Isarov, A. V.; Chrysochoos, J. *Langmuir* **1997**, *13*, 3142.
(70) Kröger, F. A. *Physica* **1940**, *7*, 1.
(71) Lambe, J.; Klick, C. C. *Phys. Rev.* **1955**, *98*, 909.
(72) Schön, M. *Zeitschrift für Physik A Hadrons and Nuclei* **1942**, *119*, 463.
(73) Klasens, H. A. *Nature* **1946**, *158*, 306.
(74) Prener, J. S.; Williams, F. E. *J. Chem. Phys.* **1956**, *25*, 361.
(75) Prener, J. S.; Weil, D. J. *J. Electrochem. Soc.* **1959**, *106*, 409.
(76) Kasai, P. H.; Otomo, Y. *Phys. Rev. Lett.* **1961**, *7*, 17.
(77) Koda, T.; Shionoya, S. *Phys. Rev.* **1964**, *136*, 541.
(78) Urabe, K.; Shionoya, S.; Suzuki, A. *J. Phys. Soc. Jpn.* **1968**, *25*, 1611.
(79) Denzler, D.; Olschewski, M.; Sattler, K. *J. Appl. Phys.* **1998**, *84*, 2841.
(80) Peng, W. Q.; Cong, G. W.; Qu, S. C.; Wang, Z. G. *Opt. Mater.* **2006**, *29*, 313.
(81) Sang, W.; Qian, Y.; Min, J.; Li, D.; Wang, L.; Shi, W.; Yinfeng, L. *Solid State Commun.* **2002**, *121*, 475.
(82) West, A. R. *Solid State Chemistry and Its Applications*; John Wiley & Sons: New York, 1984.
(83) Asano, S. *J. Phys. Soc. Jpn.* **1958**, 13.

(84) Khosravi, A. A.; Kundu, M.; Jatwa, L.; Deshpande, S. K.; Bhagwat, U. A.; Sastry, M.; Kulkarni, S. K. *Appl. Phys. Lett.* **1995**, *67*, 2702.

(85) Manzoor, K.; Vadera, S. R.; Kumar, N.; Kutty, T. R. N. *Mater. Chem. Phys.* **2003**, *82*, 718.

(86) Urabe, K.; Shionoya, S. *J. Phys. Soc. Jpn.* **1968**, *24*, 543.

(87) Suzuki, A.; Shionoya, S. *J. Phys. Soc. Jpn.* **1971**, *31*, 1462.

(88) Suzuki, A.; Shionoya, S. *J. Phys. Soc. Jpn.* **1971**, *31*, 1719.

(89) Kang, C. S.; Beverley, P.; Phipps, P.; Bube, R. H. *Phys. Rev.* **1967**, *156*, 998.

(90) Van Gool, W. Fluorescence Centers in ZnS, Philips Res. Rept. Suppl.; No. 3; Thesis; Universiteit Amsterdam, 1961.

(91) Blicks, H.; Riehl, N.; Sizmann, R. *Zeitschrift für Physik A Hadrons and Nuclei* **1961**, *163*, 594.

(92) Patel, J. L.; Davies, J. J.; Nicholls, J. E. *J. Phys. C (Solid State Phys.)* **1981**, *14*, 5545.

(93) Carter, A. C.; Bouldin, C. E.; Kemner, K. M.; Bell, M. I.; Woicik, J. C.; Majetich, S. A. *Phys. Rev. B* **1997**, *55*, 822.

(94) Chen, L.; Zhang, J.; Luo, Y.; Lu, S.; Wang, X. *Appl. Phys. Lett.* **2004**, *84*, 112.

(95) Li, Z.; Liu, B.; Li, X.; Yu, S.; Wang, L.; Hou, Y.; Zou, Y.; Yao, M.; Li, Q.; Zou, B. *Nanotechnology* **2007**, *18*, 255602.

(96) Burris, S. C.; Zhou, Y.; Maupin, W. A.; Ebelhar, A. J.; Daugherty, M. W. *J. Phys. Chem. C* **2008**, *112*, 6811.

(97) Kumar, A.; Janata, E.; Henglein, A. *J. Phys. Chem.* **1988**, *92*, 2587.

(98) Weller, H. *Angew. Chem., Int. Ed. Engl.* **1993**, *32*, 41.

JP809666T